Journal of Power Sources 269 (2014) 486–497

Contents lists available at ScienceDirect

Journal of Power Sources

journal homepage: www.elsevier.com/locate/jpowsour

# Thermo-electrochemical analysis of lithium ion batteries for space applications using Thermal Desktop

W. Walker*, H. Ardebili

*Department of Mechanical Engineering, University of Houston, 4800 Calhoun Road, Houston, TX 77004-4006, USA*

## HIGHLIGHTS

- Space environments are too complex for typical battery analysis software packages.
- Thermal Desktop is shown to be a valid orbital thermal analysis software for LIBs.
- Thermal Desktop can predict heat generation as a function of any orbital parameter.
- LIB complexities are combined with Thermal Desktop through FORTRAN programing.

## ARTICLE INFO

*Article history:*
Received 27 February 2014
Received in revised form
2 July 2014
Accepted 3 July 2014
Available online 11 July 2014

*Keywords:*
Thermo-electrochemical modeling
Lithium-ion batteries
Space applications
Orbital thermal environments

## ABSTRACT

Lithium-ion batteries (LIBs) are replacing the Nickel–Hydrogen batteries used on the International Space Station (ISS). Knowing that LIB efficiency and survivability are greatly influenced by temperature, this study focuses on the thermo-electrochemical analysis of LIBs in space orbit. Current finite element modeling software allows for advanced simulation of the thermo-electrochemical processes; however the heat transfer simulation capabilities of said software suites do not allow for the extreme complexities of orbital-space environments like those experienced by the ISS. In this study, we have coupled the existing thermo-electrochemical models representing heat generation in LIBs during discharge cycles with specialized orbital-thermal software, Thermal Desktop (TD). Our model's parameters were obtained from a previous thermo-electrochemical model of a 185 Amp-Hour (Ah) LIB with 1–3 C (C) discharge cycles for both forced and natural convection environments at 300 K. Our TD model successfully simulates the temperature vs. depth-of-discharge (DOD) profiles and temperature ranges for all discharge and convection variations with minimal deviation through the programming of FORTRAN logic representing each variable as a function of relationship to DOD. Multiple parametrics were considered in a second and third set of cases whose results display vital data in advancing our understanding of accurate thermal modeling of LIBs.

Published by Elsevier B.V.

## 1. Introduction

Increasing consumption of nonrenewable fuel and energy sources and the decreasing availability of said resources escalates the need for renewable energy, high efficiency energy consumption, transformation from reliance on non-renewable energy to renewable energy, and the incorporation of advanced energy storage technologies. The need to survive in space environments where fuel sources are not readily available also leads to an extremely high dependence on advanced energy storage capabilities. The leading advanced energy storage technologies include lithium-ion batteries, supercapacitors and hydrogen fuel cells. In considering more efficient energy storage we often consider two primary characteristics of a storage device; namely, energy density and power density. Both properties are important for optimal storage but difficult to maximize simultaneously as high energy density devices tend to have a lower power density (i.e. batteries and fuel cells) while high power density devices have lower energy density (i.e. capacitors); this type of data is typically explored by a Ragone plot. Secondary (rechargeable) and primary (non-rechargeable) lithium-ion batteries (LIBs) are increasing in popularity within industry because they prove superior over traditional batteries and other devices in energy density, power density, efficiency, operating and storage temperature ranges, life cycles, and shelf life. Studies like that by Cutchen et al. with Sandia National Laboratories [1] are primary evidence to the abilities of LIBs; the

* Corresponding author. Tel.: +1 281 483 0434.
*E-mail address:* william.walker@nasa.gov (W. Walker).

http://dx.doi.org/10.1016/j.jpowsour.2014.07.020
0378-7753/Published by Elsevier B.V.

**Nomenclature**

| | |
|---|---|
| Ah | capacity (amp-hours, Ah) |
| C | Coulombs (C) |
| $c_p$ | specific heat (J kg$^{-1}$ K$^{-1}$) |
| $E$ | working voltage (V) |
| $E_{OC}$ | open circuit potential (V) |
| $\varepsilon$ | emissivity |
| $h$ | convection (W m$^{-2}$ K$^{-1}$) |
| $H_C$ | height core section (cm) |
| $H_B$ | height total battery (cm) |
| $I$ | total current (A) |
| $K_x$ | conductivity $x$-direction (W m$^{-1}$ K$^{-1}$) |
| $K_y$ | conductivity $y$-direction (W m$^{-1}$ K$^{-1}$) |
| $K_z$ | conductivity $Z$-direction (W m$^{-1}$ K$^{-1}$) |
| $L_C$ | length core section (cm) |
| $L_B$ | length total battery (cm) |
| $\rho$ | density (kg m$^{-3}$) |
| $Q$ | heat load (W) |
| $T$ | temperature (K) |
| $T_{Ambient}$ | ambient (surrounding) temperature (K) |
| $V_{Total}$ | total volume (cm$^3$) |
| $W_C$ | width core section (cm) |
| $W_B$ | width total battery (cm) |

study by Cutchen et al. demonstrated the consistent performance of LIBs for an extended period of time (10 years) and wide temperature ranges (−40 °C to +70 °C) [1].

The National Aeronautics and Space Administration (NASA) works towards utilizing this technology for the International Space Station (ISS) by replacing Nickel–Hydrogen batteries with high performance LIBs in 2016; the primary purpose of the batteries is to store excess energy gathered by the station's solar panels for use at any given period of time. The batteries are developed by GS Yuasa Lithium Power Incorporated as a part of ISS orbital replacement units (ORUs) that are installed in the extreme vacuum environment exterior of the ISS where they will experience the large scale temperature and radiation fluctuations of space only controlled through a variety of passive (e.g. conduction and radiation) and active thermal techniques (e.g. loop heat pipes). However, LIBs face numerous challenges with the introduction of the extreme temperature orbital-space environments experienced by the ISS as the temperature variations inside a battery can significantly influence its performance, reliability and life [2,3]. When objects in orbit of Earth fly in and out of the sun's view external to a given vehicle every 45 min at 28,100 km (km) per hour (hr), as shown in Fig. 1, temperatures of said objects typically fluctuate between cold and hot extremes ranging from −150 °C to +200 °C depending on the attitude, surrounding geometries (which create conduction paths, shading, etc…), thermophysical properties, optical properties, insulation methodology, active thermal control methods and more [4]. When radiating directly to deep space, said objects (i.e. batteries) radiate to a −270 °C black body [4]. Understanding these factors and being able to accurately simulate their effects in relation to battery charge–discharge cycles is critical to thermally controlling an externally mounted LIB of any spacecraft.

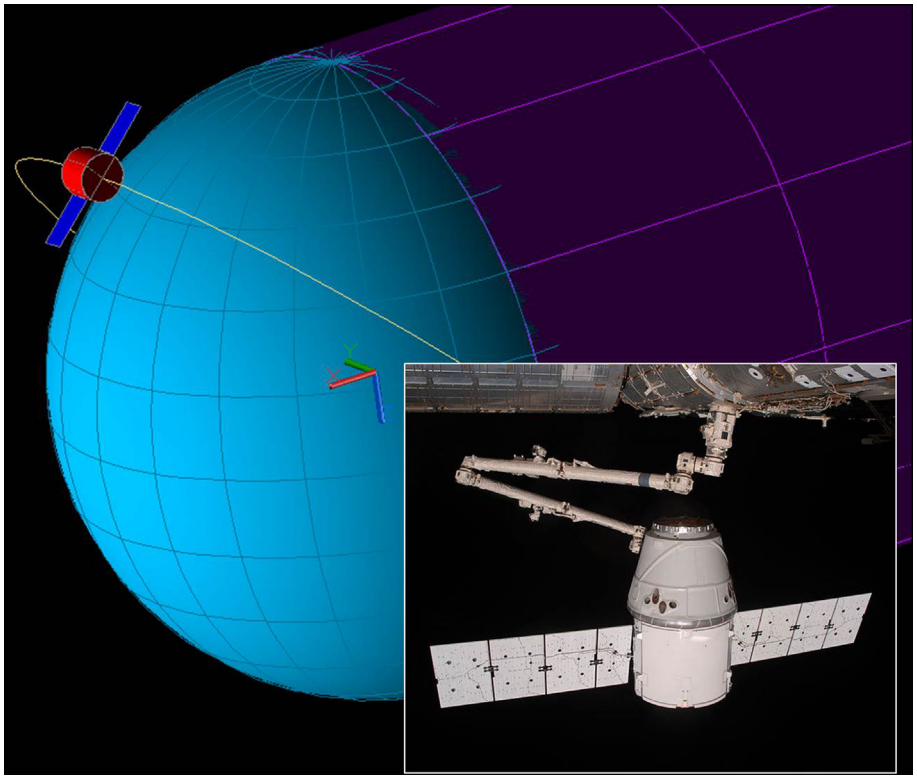

**Fig. 1.** Example orbital sequence of an object flying in and out of the sun's view and the basic factors for orbital-thermal analysis in space orbital thermal analysis software Thermal Desktop compared to a NASA taken (public) image of the SpaceX Dragon capsule berthing to the ISS via robotic mechanisms in Earth's orbit.

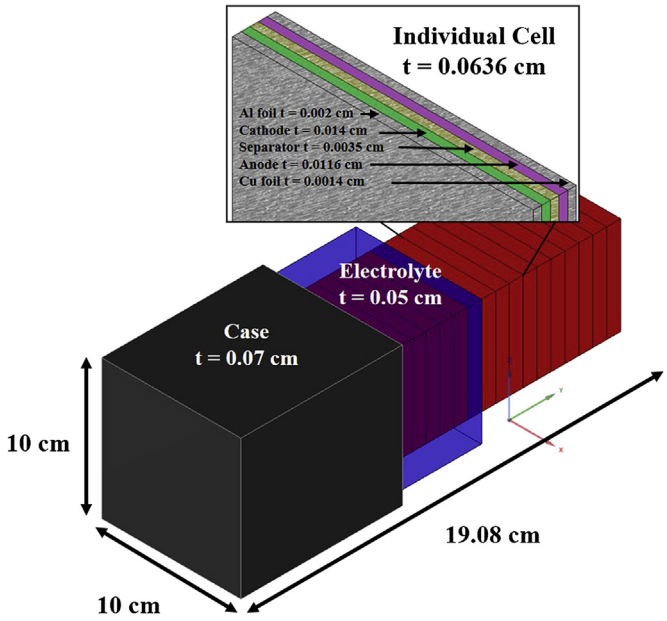


**Fig. 2.** Representation of the LIB layup used by Chen et al. [11]. The red objects represent all of the LIB cells combined into the "core" region, the transparent blue objects represent the electrolytic layer, and the gray objects represent the case.

Though advanced modeling software for batteries exists (e.g. COMSOL and CD Adapco +), these software packages are unable to incorporate the numerous complexities of the orbital-space environment, which invokes the need for specialized software. The problem is that these specialized software packages (e.g. Thermal Desktop, Siemens NX Space Systems Thermal, Thermal Synthesizer System, TRASYS, etc…) are not readily able to model the complexities of batteries. Regardless, the growing use of LIBs in space environments invokes the need to incorporate orbital-space thermal analysis software and to overcome the battery related challenges faced by said software into the battery design and validation process overall to accurately capture the thermal effects of these rapidly changing environments. In addition to the thermal effects of extreme orbital-space environments (e.g. high beta during solar summer), understanding local heating of a LIB is also critical. Local heating is generated through three primary sources in batteries; (a) interfacial kinetics, (b) species transport, and (c) joule heating caused by the movement of charged particles [2]. For larger batteries, the flow of ions from electrode to electrode and the flow of electrons through the circuit, in addition to various other parameters (i.e. the heavy dependence on surrounding temperature), all contribute to the generation of local heating. Again, these factors are easily captured in multi-physics software like COMSOL and CD Adapco+; however these software types, though they perform basic thermal analysis, are not able to completely incorporate orbital-space environments.

To ensure the success of orbit bound LIBs, this study focused on developing battery temperature prediction techniques by coupling proven numerical thermo-electrochemical models of battery reactions derived through energy balance equations with orbital-space thermal analysis software, Thermal Desktop (TD) & SINDA v5.5, to provide an intuitive orbital-space based thermo-electrochemical modeling technique. TD is a graphical user interface (GUI) incorporated into AutoCAD with tools built in that allow the user to provide thermal definition as the model is built. TD writes a FORTRAN language code as the model is built which is exported to SINDA v5.5, which solves the code for transient and steady state conditions. Once validated, this combination of space-orbital and thermo-electrochemical models would allow the charge/discharge heat generation rate of the battery to be a function of temperature for any set of orbital conditions. In that, once LIB modeling techniques are not limited to user defined environmental conditions and predefined local heat generation rates, but are coupled with present day computer processing power, the magnitude of testable cases (orbital or non-orbital) becomes countless making this coupled modeling technique extremely valuable once validated. The heat generation rate of a battery is a function of itself and the environment, and when considering orbital environments, the change in surrounding temperatures and incoming heat fluxes are far too complex to handle via simple numerical methods which invokes the need for software driven

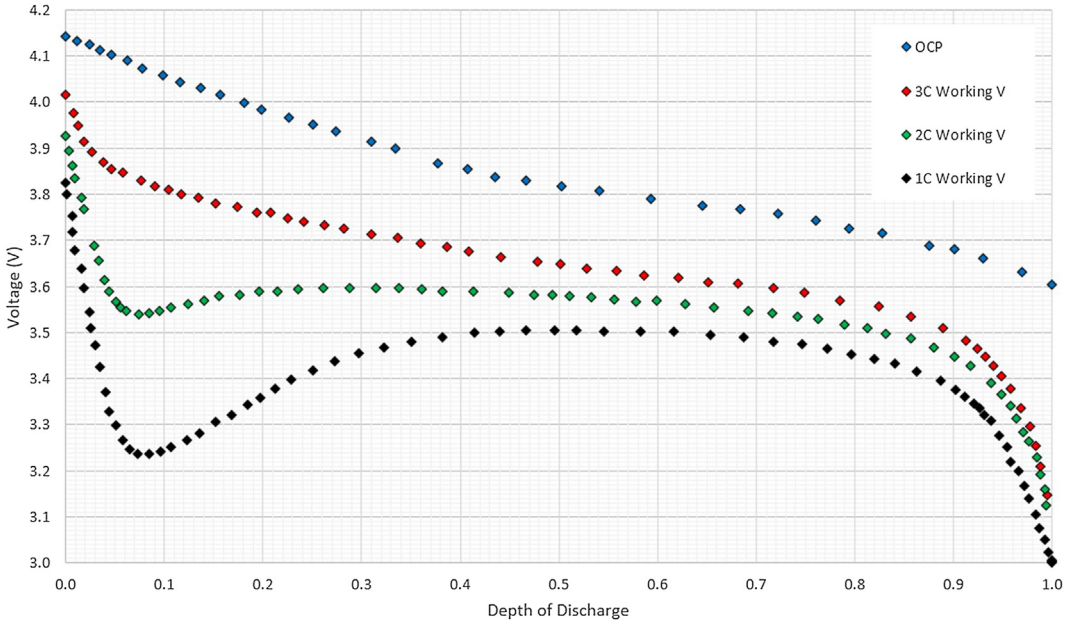


**Fig. 3.** Open circuit potential and working voltages vs. depth of discharge profiles.

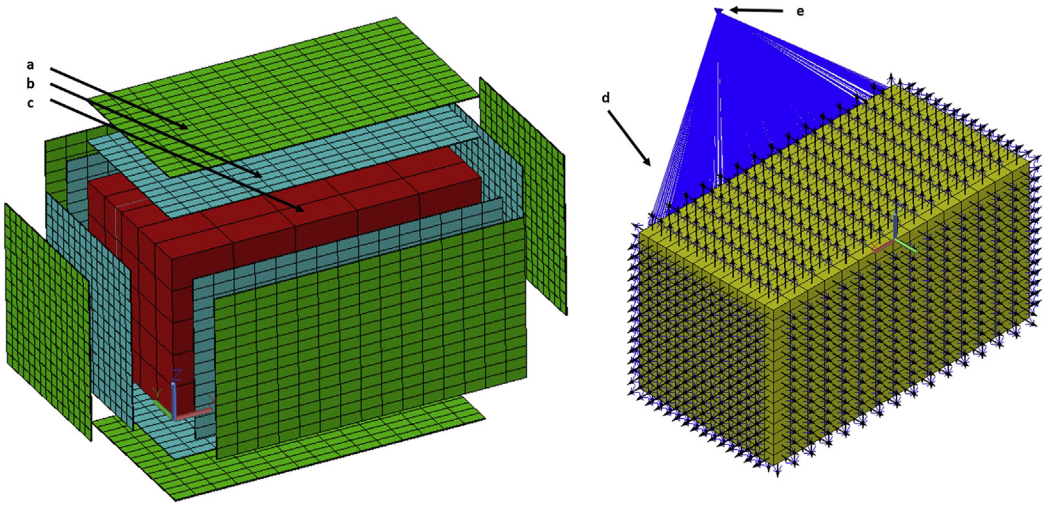


**Fig. 4.** Thermal Desktop geometries (1 solid / 12 surfaces) and elements (3825 total) representing the encasement of the LIB with convection/radiation to 300 K; (a) Encasement, (b) Electrolyte, (c) Core Region, (d) Radiation and convection application through Thermal Desktop, (e) 300 K boundary node (sink temperature).

capability. The desired end result is a LIB model in which the local heating rate is a function of the orbital model itself.

## 2. Overview of battery thermal modeling techniques

The thermal modeling of batteries can be traced back to the general energy balance equation developed by Bernardi et al. [5] in 1985. Bernardi incorporated the electrochemical reactions that occur as electrons and Li-ions flow, mixing enthalpies, and phase changes of battery systems that will be explained in greater detail in later sections. Rao and Newman [6] calculated the rate of heat generation based on the energy balance, enthalpy, and current density in 1997. Various two and three dimensional modeling studies based on these energy balance equations then followed, like those of Gu and Wang [3] who developed multi-dimensional thermal and electrochemical models of LIBs in the late 1990s and early 2000s. Chen and Evans [7–9] were also prominent in the late 1990s in developing single to multi-dimensional thermo-electrochemical battery models based on Bernardi's equations.

Throughout the mid to late 2000s, modeling studies emerged which focused on more complex characteristics such as the local heating due to mixing (Thomas and Newman, 2003, [10]) and microscale phase change passive thermal control methods (Bandhauer, 2011 [2]). These newer studies not only focused on the overall heating of the battery, but also identified the location where the heat is generated known as “hot spots”. In 2005 Chen et al. [11] developed a three dimensional convection and radiation (location dependent) model; this numerical model was chosen as the focus of the present study as they too focused on the combined effects of local heating, convection, and radiation. Chen's model examined the layered structure of cell stacks, the case of the battery pack, and the gaps between the elements. Location dependent convection and radiation were also applied – factors which are automatically implemented in Thermal Desktop. This study exemplified the importance of cooling through radiation, the effects of forced convection vs. natural convection, and the role of the encasement as a heat spreader. Studies conducted by Mills and Al-Hallaj [12] in 2005 focused not only on thermally analyzing LIB systems, but on managing the locally generated heat through phase change materials as a passive thermal management system. Numerical thermo-electrochemical models displayed that for a pack of six LIBs, for safe operation in extreme conditions, the volume needed for an appropriate amount of phase change materials would need to double showing that improved properties of the composite could lead to a reduction in volume and mass (possibly through impregnating the material with expanded graphite). Bandhauer [2] discusses the increase in heat generation at the current collector locations in his publication. In 2011 Kim et al. [13] developed methods for modeling LIB thermal behavior during the charging phases through two dimensional finite element method (FEM) simulations validated by experimental results. Specifically, the study determined the potential and current density distributions on the LIB electrodes as a function of the charging time. The charging profile consisted of constant-current followed by constant-voltage charging [13]. This study was extremely useful as it outlined the necessary methods for hot spot identification near the current collectors.

Studies in thermal, electrical, and electrochemical analysis for Lithium-ion batteries has grown immensely between 2010 and 2013. Nieto et al. [14] developed a thermal model in 2012 that represents the heat generation behavior of a large format 10.5 Ah LIB that is based on experimental measurements of internal resistance and entropic heat coefficients. Depending on the discharge rate, this model predicted to the experimental results within 15–21% error. Also in 2012, Ye et al. [15] developed numerical models which examined the electro-thermal life cycles of a LIB for various charge/discharge rates in relation to fading capacity with time. Understanding the reduction in capacity over time and accurately implementing this into thermal models is vital to the amount of accuracy the model holds. Lee et al. [16] developed a numerical model which incorporates coupled electrical and electrochemical physics for a 20 Ah large format cylindrically wound set of LIB cells. The interesting portion of these results is that because all components and materials of the battery were modeled individually, evaluation can occur at a layer to layer level which allows for the design to occur at multiple levels; number and location of tabs, thermal and electrical configuration, performance and life, etc.

Though this brief overview does not state every study that has been conducted, it does provide insight into the various topics of interest for the thermal analysis of LIBs and the techniques used by the experts in this field. More importantly, unlike the work by Kim et al. [13] most of these studies are generally numerically and experimentally driven and have not yet been fully incorporated

into all aspects of software driven geometric based thermal analysis techniques (FEM) – let alone orbital-space based thermal analysis software (TD). Clearly this lack of implementation is due to the still growing understanding of battery processes, but without implementing modern computer processing capability, researchers will not be able to maximize the number and types of cases for analysis with respect to orbital-space analysis of LIBs. It is also important to note that the use of Lithium-ion batteries in the space-aerospace industries is greatly increasing (NASA's LIB ORU system is a prime example). Private companies such as SpaceX, Boeing, and Sierra Nevada will soon dominate the near Earth orbit aspect of space travel with their manned-vehicles currently in development. Like any space vehicle superior energy storage will be key to success and LIBs offer the needed characteristics. However, without advanced analysis techniques, such as those proposed here, the design of the battery from a thermal perspective cannot be pushed to the fullest. The future use of LIBs in space-orbit environments on private vehicles will require advanced thermal prediction capability to help design a battery that is resistant to the thermal environment, a battery that is safe, and a battery that is reliable.

## 3. Thermal effects of orbital-space environments

The term “orbital-space environments” is mentioned frequently in this paper. To explain what this terminology means and the impact it has on LIB temperatures, this brief section is provided. Essentially, the ISS-orbit bound LIBs discussed in the introduction which inspired this study, like any vehicle, satellite, or body in Earth's orbit will experience a constantly changing thermal environment from launch to the end of their mission. Generally speaking the ISS travels at 28,100 km $h^{-1}$, which means an orbit is completed every 45 min based on altitude and orbit; for every orbit an object will experience a period of time in view of the sun (hot period) and a period in the Earth's shadow (cold period). LIBs have a wide range of operating and storage temperatures when considering applications on Earth, but typically have a minimum storage temperature limit of −40 °C and minimum operating limit of −20 °C which are quickly exceeded in extreme cold space environments which go well below that limit at any given point in orbit (−60 °C or colder in some cases on ISS) [4]. Typical LIBs have upper storage and operating limits between +60 °C and +80 °C, which are quickly exceeded in Earth's orbit alone (without any local heat generation effect) depending on attitude and surrounding objects; surface temperatures of objects experiencing extreme orbits can reach +200 °C or more. The combination of a hot attitude with strong LIB local heating could lead to thermal runaway if the performance of the battery at any point in orbit is not fully understood.

Several primary factors come into consideration when determining the thermal performance of a battery in orbital environments; (a) attitude, (b) battery thermophysical and optical properties, (c) conduction paths and (d) surrounding structures. The attitude of any object in orbit is defined by various categories [17]: Yaw, pitch, and roll are the *x*, *y*, and *z* rotation of the orbiting object, beta angle is the angle between the solar vector and it's projection onto the orbit plane, solar flux is the intensity of the incoming radiation energy from the sun, albedo heating is the solar energy reflected from the planet and its atmosphere, infrared flux is the heating in the infrared spectrum from the planet called planetary outgoing long-wave radiation, and orbital velocity is the velocity that the object orbiting the planetary body in its orbital vector which will dictate how long the object is in the sun and out of the sun.

Typical thermophysical properties considered are thermal conductivity (W $m^{-1}$ $K^{-1}$), specific heat (J $kg^{-1}$ $K^{-1}$) and density (kg $m^{-3}$). These properties combined with local heating and the environment determines how quickly or slowly an object heats up or cools down. Specific heat and density are often not focused on when steady state computations are performed since these two dictate the rate of heat up or cool down, but because of the completely transient nature of the thermal assessment of a LIB they are very important. Optical properties focused on are surface absorptance ($\alpha$) and surface emittance ($\varepsilon$). These properties dictate how the object emits, absorbs, transmits, and conducts thermal energy. Measuring and using the exact optics in an analysis is vital when considering the impact these properties play when combined with solar radiation, albedo, etc. For example, if a given LIB has an encasement with an extremely low emittance (e.g. 0.03), the surface temperatures can quickly exceed +200 °C whereas the same battery with a higher emittance (e.g. clear anodized aluminum 0.87 [4]), the surface temperatures may remain around +80 °C. Typically radiation is not a major driver of thermal control for a battery, but in space where radiation is one of the only primary forms of passive thermal control, radiation becomes far more important. Also note that Chen et al. reports that even on Earth in a convective environment that controlling surface optics of the encasement can attribute to 28–30% of the cooling of a given battery [11].

For orbital environments, energy gain/loss through convection would be nonexistent unless by conduction to some type of active cooling technique. Conduction will occur through the solids (and/or semisolids) of the system in itself and at the mounting locations to the primary body in orbit as long as that body is cooler than the battery. The rate at which energy is gained/lost at this contact location is dependent on how well the objects are in contact; i.e. how much thermal resistance exists (conductance).

In addition to the attitude and thermophysical properties, the surrounding structures and mounting location of the orbiting object play a major role in understanding the thermal environment as these objects provide shading (or no shading) which increase or decrease the thermal energy experienced by the system. For this reason it is imperative that specialized software like TD are used which take into account the changes in shading at any given point in orbit; see Fig. 1.

Zero gravity and vacuum environments also play a role. Microgravity, often referred to as zero-gravity, and vacuum means that natural convection will not be present to cool the system as stated previously [4]. It should be noted that the effects of vacuum and 0-G could alter the movement of ions, electronics, etc. which would not only affect the efficiency of the battery, but would also affect the rate at which local heating occurs. Because so many factors are considered during orbital analysis, even with modern computing capability, the complexity of these models drives up the computation time. Therefore, once a baseline model (non-orbital) is developed by this study within the orbital-thermal analysis software and validated, the analysts could then incorporate all factors of orbital heating as described in this section into the definition of a battery's local heating and as the definition of the battery's environment; trouble-shooting would take far too long if doing so on an orbital model.

## 4. Lithium-ion battery charge/discharge heating and heat transfer mechanisms

Lithium-ion batteries mainly comprise of two electrodes (an anode and a cathode), an electrolytic material and separator between the electrodes, and current collectors on both electrodes. Ion and electron movements occur simultaneously as the electrochemical reaction progresses between the electrodes when a potential is applied. Generally speaking, LIBs are highly regarded among other batteries due to characteristics such as high cell

voltage, flat discharge rate, long shelf life (which is extremely useful for long duration space flight applications), cyclability, wide operating temperature range, high energy density and high power density. However, despite these impressive energy storage characteristics, LIBs are weighted with major thermal problems, such as thermal runaway and poor low temperature limits in respect to space environments; problems that are compounded with the addition of complex orbital-space temperatures. As previously stated, not only are cell temperatures a function of the surrounding environment, but also are a function of the movement of ions and electrons which generate heating as a function of surrounding temperatures, velocity of the electrons/ions, the total potential, battery efficiency, solid electrolyte interphase (SEI), dendrite growth and the battery material properties [11].

This combination of orbital parameters and local heating rates can lead to loss in capacity, efficiency, and to thermal runaway in worst hot cases. Thermal runaway, the primary thermal concern for most LIBs, has caused buses, taxis, other vehicles, and computers and other mobile devices to catch fire or explode which presents strong reasoning for the need to thoroughly understand the combined effects of orbital heating and battery local heating [18]. To prevent these types of failures, engineers incorporate modeling to assist in the design process where a large variety of environmental, material properties, charge, and discharge parameters are considered in various combinations. However, due to the extremely complex nature of batteries and the countless variables that affect thermal profiles, even modeling has its limits. The local temperatures of a battery are affected by convection, conduction, radiation, and local heating. Convection, conduction, and radiation are clearly defined modes of heat transfer as described by Equations (1)–(3) respectively (note that convection is used in this study to replicate Chen's test setup, but will not be needed when simulating the vacuum environment of space in future studies; even if the battery was inside the vehicle where air was present, convection would be minimal as a microgravity environment prevents natural convection and airflow speeds through the vehicle would be low.):

$$Q_{\text{Conv}} = hA\left(T_{\text{Surface}} - T_{\text{Environment}}\right) \tag{1}$$

where $h$ is the convection heat transfer coefficient (W m$^{-2}$ K$^{-1}$), $A$ (m$^2$) is the surface area, $T_{\text{Surface}}$ (K) is the temperature of the surface, and $T_{\text{Environment}}$ (K) is the temperature of the surrounding environment.

$$Q_{\text{Cond}} = -kA\frac{\mathrm{d}T}{\mathrm{d}x,y,z} \tag{2}$$

where $k$ is the thermal conductivity (W m$^{-1}$ K$^{-1}$), $A$ (m$^2$) is the surface area, $dT$ (K) is the change in temperature between two points through the solid, and $d_{x,y,z}$ is the distance between the two points.

$$Q_{\text{Rad}} = \varepsilon\sigma AF\left(T_{\text{Hot}}^4 - T_{\text{Cold}}^4\right) \tag{3}$$

where $\varepsilon$ is the surface emissivity, $\sigma$ is Stefan–Boltzmann constant, $A$ (m$^2$) is the surface area, $F$ is the form factor between the radiating surface and the radiation sink, and $T$ (K) is the temperature of the respective surfaces. Though radiation is not typically considered a major thermal driver for battery thermal analysis, Chen's study displayed that radiative heat transfer as a function of encasement surface optical properties attributes to 28–30% of the cooling a battery [11]. Even if radiation isn't a major thermal driver on Earth, it is the only passive method (aside from conduction to an active cooling/heating device) for heat transfer to occur in the vacuum of space.

Generally speaking, the local heating rate of a battery is based on a series of energy balance equations over a "representative elementary volume, REV" developed by Bernardi et al. [5]. The local heating of the REV is represented Equation (4) which Bernardi et al. derived by applying the first law of thermodynamics for an isobaric battery, thermodynamic properties of the reactions, the potential-current characteristics of the cell, and the rates of charge–discharge to a control volume, or REV (equation includes current, working voltage, open circuit potential, phase change terms and enthalpy of mixing) [5]:

$$Q_{\text{Local}} = -IV - \sum_k I_k T^2 \frac{\mathrm{d}\frac{U_{k,\text{avg}}}{T}}{\mathrm{d}T} + \sum_j \frac{\mathrm{d}}{\mathrm{d}t}\left(\int_{v_i}\bar{\sum_i} c_{ij} RT^2 \frac{\partial}{\partial T}\ln\left(\frac{y_{ij}}{y_{ij}^{\text{avg}}}\right)dv_j\right) + \sum_{jjm}\sum_i\left[\left(\Delta H_{ij\to m}^* - RT^2\frac{\mathrm{d}}{\mathrm{d}T}\ln\left(\frac{\gamma_{i,m}^{\text{avg}}}{\gamma_{i,j}^{\text{avg}}}\right)\right)\frac{\mathrm{d}n_{i,j}}{\mathrm{d}t}\right] \tag{4}$$

In general the first term is the electrical power from the battery, the second term is the sum of available work and entropic heating, the third term is the heat produced from mixing, and the last term is the heat associated with material phase changes [11]. This equation is also utilized consistently in a simplified form, Equation (5), which captures heat due to Ohmic losses, charge-transfer at the interface, and mass transfer limitations [2]:

$$Q_{\text{Local}} = I\left(E_{\text{OC}} - E - T\frac{\partial E_{\text{OC}}}{\partial T}\right) \tag{5}$$

where $I$ is the total current, $E_{\text{OC}}$ is the open circuit potential, $E$ is the working voltage, $T$ is the temperature, and $\partial E_{\text{OC}}/\partial T$ is the change in open circuit potential with the change in time. Phase change and mixing effects are negated with the assumption that there is only one electrochemical reaction in the battery cell (during normal operation phase change does not occur in LIBs and only one reaction occurs) [2]. Chen et al. [11] explains that Equation (5) is efficient enough for overall temperature prediction and does not limit the ability to perform accurate thermal analysis despite its simplifications from (4), and further uses (5) to predict 3-D core temperatures for various discharge processes of a 185 Ah battery. This form of Bernardi's equation, divided volumetrically, is commonly used for the thermal analysis of LIBs; examples being the three-dimensional battery pack studies by Sun et al. [19] and the studies of cylindrical LIB discharge cycles by Jeon and Baek [20]. As with the provided example studies, correctly incorporating Equation (5) into orbital-space thermal analysis software for a local heating rate of a REV is the focal point and ultimate goal of this study.

## 5. Thermal Desktop model development

A thermo-electrochemical model of a series of experiments by Chen et al. [11] for a large scale 185 Amp-Hour (Ah) LIB experiencing a 60 min discharge at 185 A (1 C) in a first test, a 30 min discharge at 370 A (2 C) in a second test, and a 20 min discharge at 555 A (3 C) in a third test, discharged continuously, for both forced and natural convection environments at 300 K was recreated in finite element form in TD & SINDA v5.5 as a baseline thermal model to determine the compatibility of the orbital-space and radiation based software for thermo-electrochemical analysis. This section discusses the development of the geometries, the application of local heating to a REV, thermophysical properties (thermal conductivity, specific heat, and density), surface optical

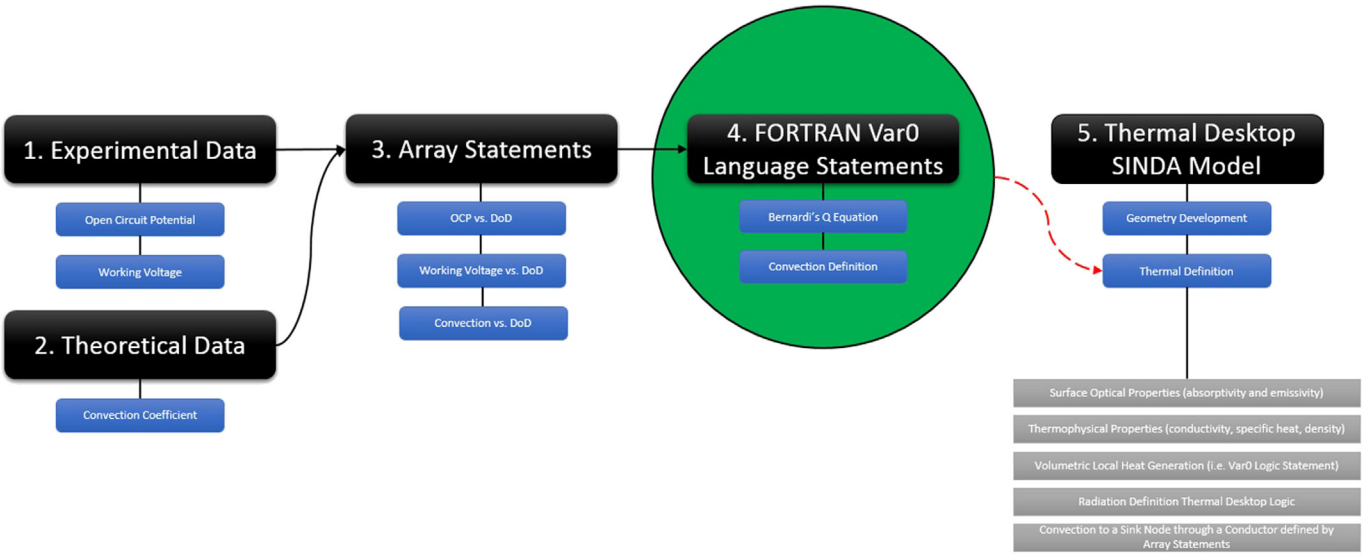


**Fig. 5.** Process flow diagram describing the process of developing a Thermal Desktop model with LIB local heat generation programed as a function of depth of discharge. Experimental data provides the open circuit potential and work voltages for depth-of-discharge. Theoretical convection data based on vertical and flat plates is determined. Experimental and theoretical data define array statements of value vs. depth-of-discharge which feed into FORTRAN Var0 statements (variable statements) for convection and Bernardi equation application. These array statements are set as definitions in TD for the geometry representing the core region.

properties, the institution of environmental parameters (convection and radiation), and the test case matrix. The development of the model as a whole is represented at the end of this section with Fig. 5.

### 5.1. Geometry development and assigned material properties

The model consisted of thee primary sub-models: the metal encasement that serves as a heat spreader, the core region (representation of the cells), and the contact layer that represents the electrolytic layer between the case and the core region. Fig. 2 is a representation of the basic battery layup considered for this analysis. These geometries were imported into TD v5.5 where nodalization and thermal definition were provided. The battery encasement was represented in Thermal Desktop with 1233 nodes and 6 individual solids that were assigned a thickness of 0.07 cm, Aluminum thermophysical properties, and an exterior surface emittance of 0.25 for radiative purposes. The electrolytic contact region is represented with 1233 nodes and 6 solids that were assigned a thickness of 0.05 cm and electrolytic material properties. A solid block represents the core region that we subdivided into five nodes along the length ($x$-axis) and five nodes in the y-z axes to yield a total of 125 nodes. Essentially the thermophysical properties of the core region in TD is a lump mass of averaged properties representing all of the individual cells of Chen's battery combined as Chen et al. did with their model [11]; since Bernardi's equations consider the overall heat generated by the total battery core region volumetrically, material properties (i.e. all of the cells combined), and voltage, this simplification was acceptable. This solid block was assigned anisotropic thermophysical properties based on the properties of cell materials (electrodes, foils, the separator, and current collectors). The reader should note that Chen et al. [11] did not include an electrolytic layer between the electrodes of each cell, but instead considered an electrolytic layer that surrounds the exterior of all of the packaged cells resulting in a slightly increased anisotropic thermal conductivity values; these effects are discussed in detail later. The completed TD model consisted of 3825 nodes divided between 13 solid elements; a relatively small model for modern computational resources (see Fig. 4 in Section 5.3). Table 1 describes all dimensions and other physical characteristics translated from Chen's analysis into the TD model.

### 5.2. Local heating

Each of the 125 core region nodes are assigned a local volumetric $q$ value based on Equation (5). Bernardi's equation, in its most basic form, provides a total volumetric heat rate of the core region of a given battery in W cm$^{-3}$. To apply this heating rate correctly TD logic was established to apply individual $q$ values to each of the 125 core region nodes based on (5) and then to multiply this value by 15.3 cm$^3$ (the volume that each node represents). The total volume of the core region is 1908 cm$^3$, or approximately 125 individual blocks of 15.3 cm$^3$. The voltages of Bernardi's equation ($E_{OC}$ and $E$) were based on experimental data gained from Chen et al. [11]. The experimentally determined curves for the 185 Ah LIB for 1 C, 2 C, and 3 C discharge rates are represented in Fig. 3 as a function of voltage vs. depth of discharge (DOD). Because TD v5.5 works with power applications as functions of time rather than DOD, arrays of these curves with respect to time were developed representing the following: 1 C = 60 minutes discharge time ($I$ = 185 A for 60 min discharge time), 2 C = 30 minutes discharge time ($I$ = 370 A for 30 min discharge time), and 3 C = 20 minutes discharge time ($I$ = 555 A for 20 min discharge time).

### 5.3. Environmental and contact region characteristics

The external surfaces were set to radiate to a constant sink temperature of 300 K and were also exposed to boundary node set to a constant 300 K via a conductor with convection values ranging from 4.25 to 10.55 W m$^{-2}$ K$^{-1}$ depending on location (location dependent natural convection values were provided by Chen et al.). A representation of the TD version of the convection and radiation network is shown in Fig. 4.

Two locations of contact existed in this model; between the encasement bottom and the top of the contact region solids and between the bottom of the contact region and the top of the core region block. Chen et al. noted that thermal resistance between all contacting surfaces should be negligible because the electrolytic

**Table 1**
Physical characteristics of the model.

| Characteristic | Value | Unit |
|---|---|---|
| Total battery dimensions | 19.32 × 10.24 × 10.24 | cm × cm × cm |
| Thickness of the case | 0.07 | cm |
| Thickness of the electrolytic layer | 0.05 | cm |
| Core region dimensions (cells combined) | 19.08 × 10 × 10 | cm × cm × cm |
| Individual cell dimensions | 0.0636 × 10 × 10 | cm × cm × cm |
| Thickness of the Al foil | 0.002 | cm |
| Thickness of the Cu foil | 0.0014 | cm |
| Thickness of the cathode | 0.014 | cm |
| Thickness of the anode | 0.0116 | cm |
| Theoretical capacity | 185 | Ah |
| Surrounding temperature | 300 | K |
| Initial temperature | 300 | K |

solution surrounded the core and was filled to all edges of the encasement. Also note that prior to testing, the core region was allowed to soak in the electrolytic material prior to any testing to allow the solution to fill any gaps and pores [11]. In Thermal Desktop a conductance value of 3000 W $m^{-2}$ $K^{-1}$ (high conductance = low thermal resistance) was assumed at both regions of contact (an arbitrarily high and typically used value for negligible thermal resistance in Thermal Desktop models when defining contactors between surfaces). Table 2 describes the averaged material properties of the core region, the material properties of the encasement, and the properties of the contact region (the electrolytic material) as defined by Chen et. al. [11].

### 5.4. Three cases analyzed

In this study, three cases were analyzed: Case 1 (replication study), Case 2 (model improvement), and Case 3 (parametric of parameters). In Case 1, a replication of Chen's study was conducted – the same $E$ and $E_{OC}$ profiles and a constant 300 K local $T$ value applied to Bernardi's equation for local heating. Case 2 sought to improve the model provided by Chen et al. through the implementation of the $E$ and $E_{OC}$ arrays and TD logic to update the local temperature value after each iteration. With said logic implemented, as the local temperature would update per iteration the overall $q$ value for the node varied as a function of DOD – though the effect was small as expected because $T$ is multiplied against an $e$-4 variable. Case 3 considered a small parametric study to observe the effects of different combinations of increased/decreased core region $\rho$, and core region $c_p$; the inspiration for this examination was because it was noted previously that Chen did not account for the fact that an electrolytic layer typically exists between the two electrodes (Chen's calculations did not include the electrolyte in the core region material properties calculations). Table 3 describes all test cases analyzed.

## 6. Results and discussion

The completed model is executed on a 12-Core workstation (core count directly decreases calculation time in the SINDA solver that Thermal Desktop feeds into) with 16 GB RAM (RAM availability is directly associated with the length of time associated with radiation calculations) and takes less than 30 s to finish – a relatively small model for Thermal Desktop. Results are provided in the following sections for Case 1, Case 2 and Case 3. Again, the goal of Case 1 was to replicate the numerical assessment conducted by Chen et al. in Thermal Desktop, Case 2 sought to examine possible improvements to the modeling technique by programming model logic to update Q as a function of temperature for every iteration of the model, and Case 3 provided a parametric investigation of the effects of different material property combinations.

**Table 2**
Thermophysical properties of the model [11].

| Material | Density (kg $m^{-3}$) | Specific heat (J $kg^{-1}$ $K^{-1}$) | Thermal conductivity (W $m^{-1}$ $K^{-1}$) |
|---|---|---|---|
| Carbon electrode | 1347.3 | 1437.4 | 1.04 |
| $LiCoO_2$ electrode | 2328.5 | 1269.2 | 1.58 |
| Al foil | 2702 | 903 | 238 |
| Cu foil | 8933 | 385 | 398 |
| PP separator | 1008.9 | 1978.2 | 0.33 |
| Al-2024 | 700 | 477 | 14.6 |
| Electrolyte | 1129.9 | 2055 | 0.60 |

### 6.1. Case 1 results (replication study)

For Case 1, an exact replication of Chen's study was created in TD. Logic was programmed into TD to update the battery's $q$ value constantly throughout TD's solving process based on changes in open circuit potential and working voltage through depth of discharge. A constant 300 K value was applied to the temperature variable of Bernardi's equation and the model convected-radiated to a 300 K sink temperature. This variation of the model was executed for the three discharge rates and six convection rates as applied in Chen's study; see Fig. 6 for the 1–3 C discharge at natural convection results and Fig. 7 for the 3 C discharge with forced convection.

The results of our TD simulation for Case 1 (replication of Chen's model) follows that of Chen's both in the transient temperature profiles and the end of cycle profiles with minimal deviation. The "hot spot" location for the TD results was found to be the same as that described by Chen et al.; towards the middle in the $x$-axis direction and slightly from the top in the $y$–$z$ directions as a result of the high heat capacity and low thermal conductivity of the electrolytic solution and the high thermal conductivity of the encasement which acts as a heat spreader. The isotherm of the core section is displayed in Fig. 8. The results from Case 1 alone, compared to Chen et al., successfully demonstrate that TD & SINDA

**Table 3**
Case matrix.

| Case ID | Case type | Discharge rate (C) | Total discharge time (s) | Current (A) | Convection (W $m^{-2}$ $K^{-1}$) |
|---|---|---|---|---|---|
| C1-3C-NAT | Case 1 | 3 | 1200 | 555 | Natural |
| C1-2C-NAT | Case 1 | 2 | 1800 | 370 | Natural |
| C1-1C-NAT | Case 1 | 1 | 3600 | 185 | Natural |
| C1-3C-20 | Case 1 | 3 | 1200 | 555 | 20 (Forced) |
| C1-3C-50 | Case 1 | 3 | 1200 | 555 | 50 (Forced) |
| C1-3C-100 | Case 1 | 3 | 1200 | 555 | 100 (Forced) |
| C1-3C-200 | Case 1 | 3 | 1200 | 555 | 200 (Forced) |
| C1-3C-300 | Case 1 | 3 | 1200 | 555 | 300 (Forced) |
| C2-3C-NAT | Case 2 | 3 | 1200 | 555 | Natural |
| C2-2C-NAT | Case 2 | 2 | 1800 | 370 | Natural |
| C2-1C-NAT | Case 2 | 1 | 3600 | 185 | Natural |
| C2-3C-20 | Case 2 | 3 | 1200 | 555 | 20 (Forced) |
| C2-3C-50 | Case 2 | 3 | 1200 | 555 | 50 (Forced) |
| C2-3C-100 | Case 2 | 3 | 1200 | 555 | 100 (Forced) |
| C2-3C-200 | Case 2 | 3 | 1200 | 555 | 200 (Forced) |
| C2-3C-300 | Case 2 | 3 | 1200 | 555 | 300 (Forced) |
| C3-Cp1 | Case 3 | 3 C discharge, natural convection, 0.85% specific heat, actual density | | | |
| C3-Cp2 | Case 3 | 3 C discharge, natural convection, 0.90% specific heat, actual density | | | |
| C3-Cp3 | Case 3 | 3 C discharge, natural convection, 0.95% specific heat, actual density | | | |
| C3-Cp4 | Case 3 | 3 C discharge, natural convection, 1.05% specific heat, actual density | | | |
| C3-Cp5 | Case 3 | 3 C discharge, natural convection, 1.10% specific heat, actual density | | | |
| C3-Cp6 | Case 3 | 3 C discharge, natural convection, 1.15% specific heat, actual density | | | |

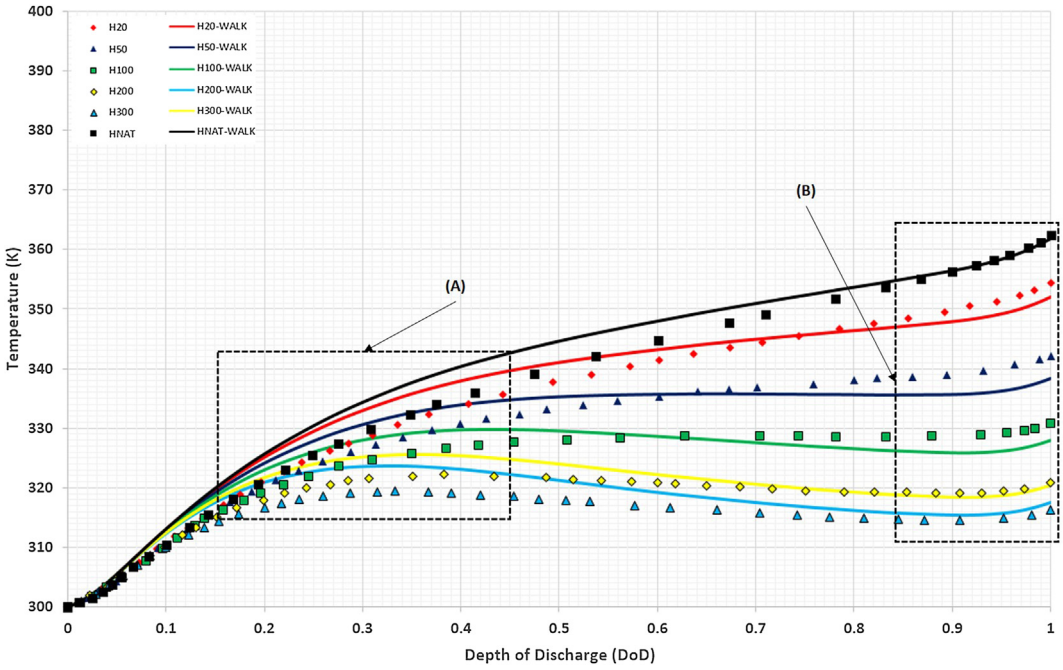


**Fig. 6.** TD results for 185.3 Ah LIB Case 1 compared to Chen's results for forced convection. (A) Location of largest error at DOD 0.15 to 0.45 (1.4% based on 4.5 K difference between actual and predicted). (B) Accurate transient predictions in general and strong correlation to end of cycle reality.

v5.5 do have the capability to accurately simulate LIB local heating through discharge; the observed slight prediction differences are due to software solver type differences and input variation for parameters that were not directly specified – minimal imperfections are understandable when comparing results from different prediction sources.

### 6.2. Case 2 results (updated local temperatures in Q calculation)

Case 2 analyses sought to improve Chen's model, which assumed a constant 300 K for $T$ in Bernardi's equation. Logic was programmed into TD to update the battery's $q$ value constantly throughout TD's solving process based on changes in open circuit potential, working voltage, and local temperature (rather than a constant 300 K) through depth of discharge. This variation of the model was executed for all discharge rates and convection types conducted by Chen's numerical analysis for comparison and results are displayed in Fig. 9 (forced convection) and Fig. 10 (natural convection).

The results indicate that for the temperature profile at the end of cycle transient for all discharge cases were approximately 1 K lower than the model without the updating T. Based on Bernardi's

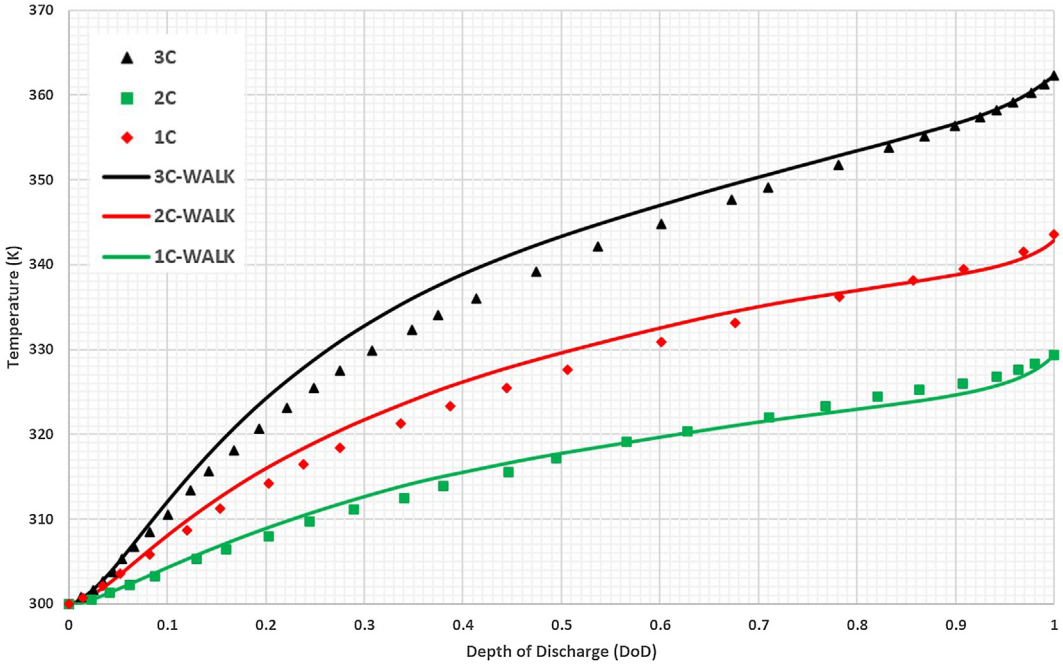


**Fig. 7.** TD results for 185.3 Ah LIB Case 1 compared to Chen's results for natural convection. Location of largest error the same as with forced convection results.

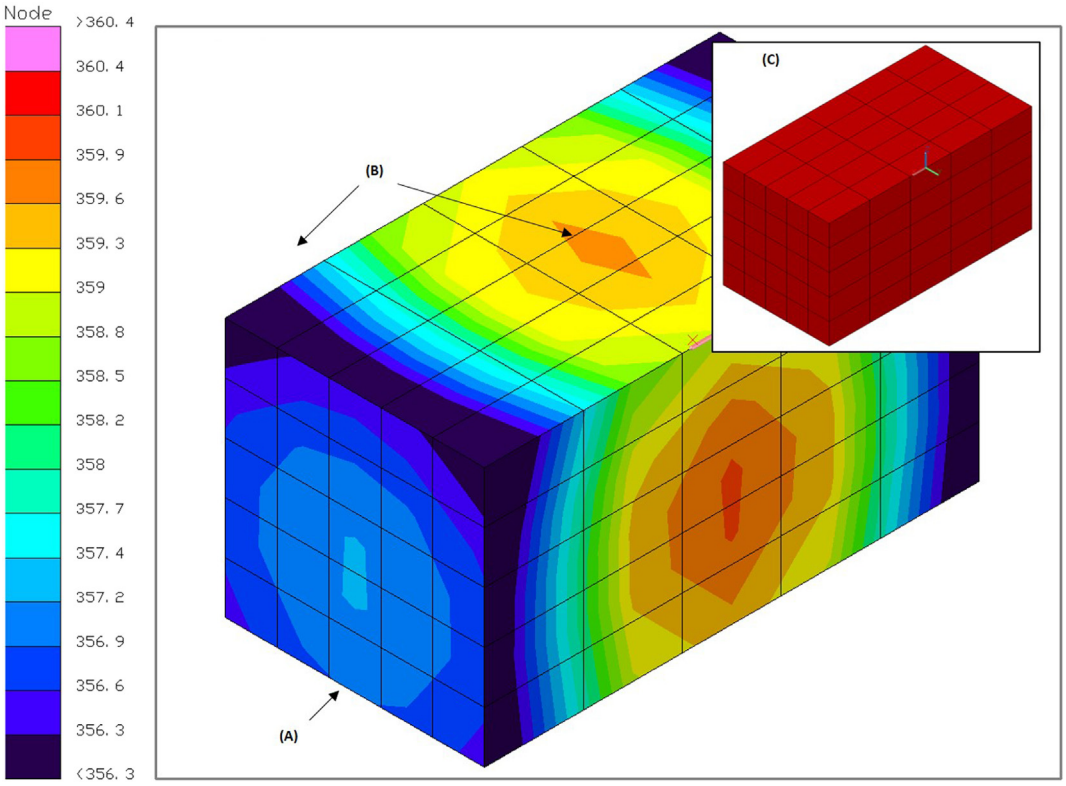


**Fig. 8.** Isotherm of core section results for Case 1 3 C discharge and natural convection. (A) Effects of lower convection coefficient on the base of the encasement are captured. (B) Cooler edges and a warmer center as an effect of a low $k_x$ and high $k_{yz}$. (C) Non-post processed core region nodes.

$Q$ equation it is observed that this lower temperature profile appears to be highly sensible as it decreases the total voltage that the volumetric current is multiplied against. For a general sink temperature analysis, Chen's model assumption would make for a slightly more conservative assessment. The reader should note that this is an effect of the battery radiating–convecting to only a 300 K sink. The effect of a higher local temperature in non-symmetric locations through the entirety of DOD as a result of simultaneous hot orbit and shading (e.g. +75 beta angle, hot solar environment, etc…) could drastically alter the transient profile more than just a degree; the isotherm through DOD could be completely different as well. The authors recognize that the updated/iterated temperature is multiplied against an $e$-4 value that alone is almost negligible – this study simply recommends that this parameter not be neglected, but considered a combined effect with orbital heating.

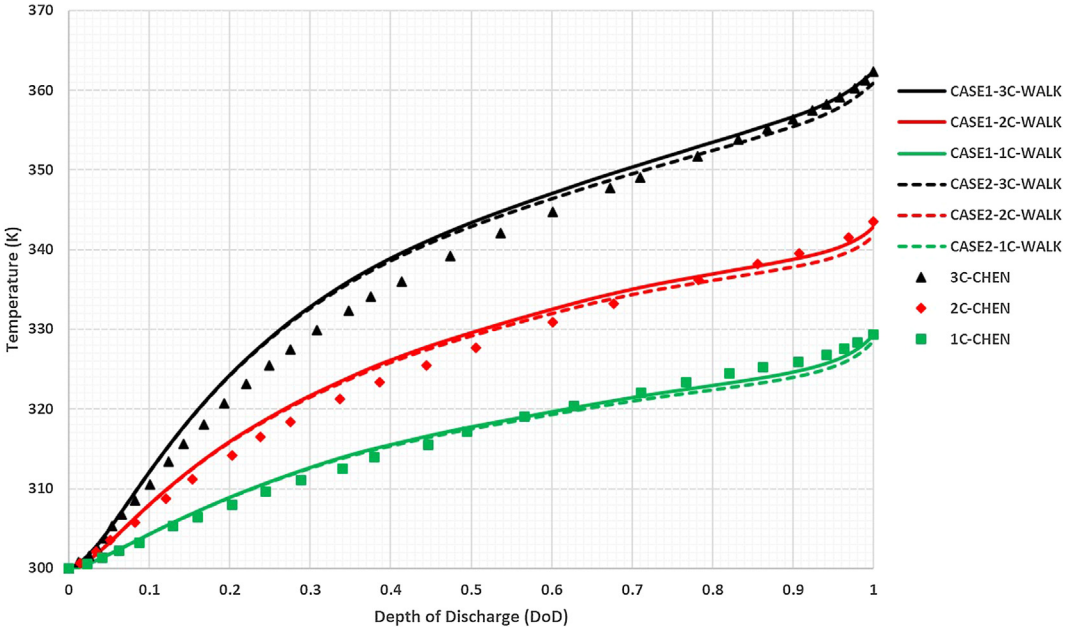


**Fig. 9.** TD results for 185.3 Ah LIB Case 2 for natural convection.

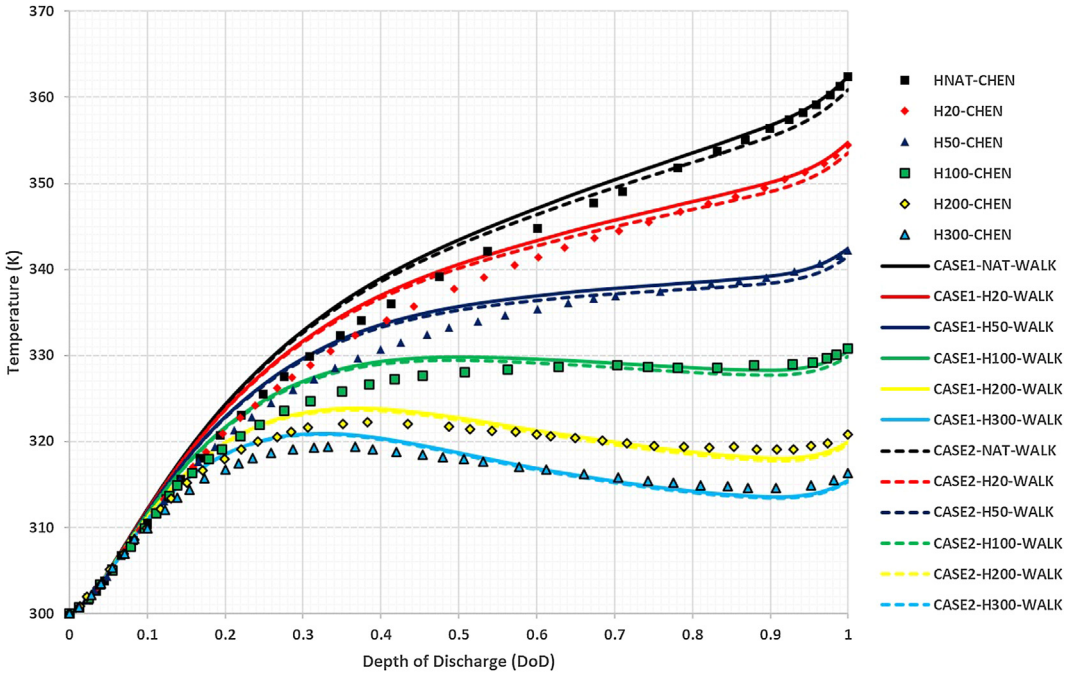


**Fig. 10.** TD results for 185.3 Ah LIB Case 2 for forced convection.

### 6.3. *Case 3 results (parametric of material properties combinations)*

Case 3 was inspired when it was noted that Chen's battery did not directly include an electrolytic layer between the electrodes which in sensibly was not included for their calculations of *x*, *y*, *z* core region material properties. This circumstance presented the question: what is the effect on the transient thermal profile as a result of error related calculations in core section specific heat and density? For Case 3, six combinations of core section thermo-physical properties were considered (note that only specific heat was varied – varying density by the same percentages would yield the same transient effects); (a) 15% $C_p$ reduction with actual $\rho$, (b) 10% $C_p$ reduction with actual $\rho$, (c) 5% $C_p$ reduction with actual $\rho$, (d) 5% $C_p$ increase with actual $\rho$, (e) 10% $C_p$ increase with actual $\rho$, (f) 15% $C_p$ increase with actual $\rho$. These cases are summarized in Table 3.

As volume averaged properties play a significantly important role in this modeling technique, these variations explore the effects that are caused by incorrect calculation/determination of the combined material properties (the effects of user error). These

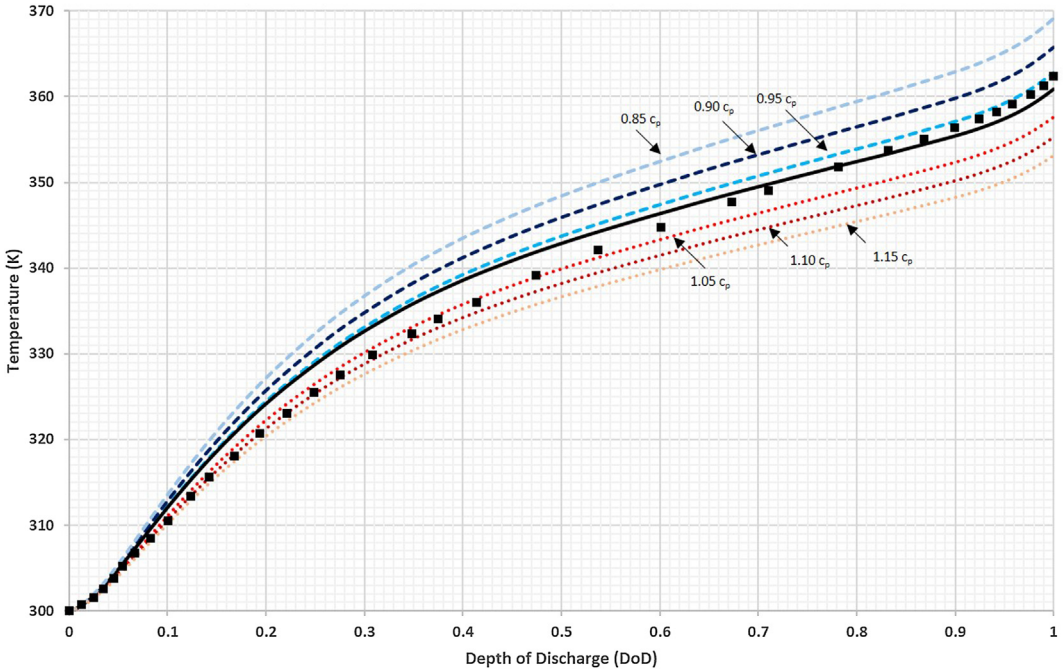


**Fig. 11.** TD results for 185.3 Ah LIB with core section $c_p$ variations implemented (3 C natural convection).

different property combinations were considered for a constant 3 C discharge rate of the 185.3 Ah LIB with natural convection. The results in Fig. 11 exemplify the importance of implementing the correct thermophysical properties into the model and the effects of even slight properties calculation error could have on the predicted results. Overestimating core region $c_p$ results in lower predicted temperatures while underestimating results in higher predicted temperatures.

## 7. Conclusion

In this study, we validated the capability of orbital-space thermal analysis software Thermal Desktop with being coupled with thermo-electrochemical reaction energy balance equations for a combined model. Case 1 results displayed accurate replication of the temperature profiles provided by Chen et al. for all discharge and convection combinations which supports the use of TD & SINDA v5.5 for orbital-space thermo-electrochemical analysis of LIBs. Any deviation from actual values, which as shown previously is minimal, would easily be encompassed by recommended predicted +11 °C margin for test correlated thermal models recommended by the widely used Gilmore Satellite Thermal Control Handbook and in the Department of Defense Standard Practice Product Verification Requirements for Launch, Upper Stage, and Space Vehicles (MIL-STD-1540D) section for thermal model margin for spacecraft hardware [4,21]. Case 2 identified the impact of updated local temperature in the Bernardi equation on local heat generation as an additional function of the model; that for less extreme sink temperatures and heat fluxes the change in heat generation is minimal, but that combination with space environments could greatly affect the transient thermal profile and isotherms. Case 3 results displayed the impact of varying thermophysical properties on the overall result and exemplify that even minimal error in core region property calculation could have a devastating effect on predictions (e.g. the prediction of temperatures lower or higher than what the battery will actually experience).

## Acknowledgments

The authors would like to give a special thanks to the support of the Thermal Design Branch at NASA Johnson Space Center for assistance with Thermal Desktop and SINDA v5.5.

## References

[1] J. Cutchen, A. Baldwin, S. Levy, J. Power Sources 14 (1985) 167–172.
[2] T. Bandhauer, S. Garimella, T. Fuller, J. Electrochem. Soc. 158 (3) (2011).
[3] W. Gu, C. Wang, J. Electrochem. Soc. (2000).
[4] D. Gilmore, Satellite Thermal Control Handbook, The Aerospace Corporation Press, El Segundo, CA, 1994.
[5] D. Bernardi, E. Pawlikowski, J. Newman, J. Electrochem. Soc. 132 (4) (1985).
[6] L. Rao, Newman, J. Electrochem. Soc. 144 (1997) 2697.
[7] Y. Chen, J. Evans, J. Electrochem. Soc. 140 (1993).
[8] Y. Chen, J. Evans, J. Electrochem. Soc. 141 (1994) 2947–2955.
[9] Y. Chen, J. Evans, J. Electrochem. Soc. 143 (1996) 2708–2712.
[10] K. Thomas, Newman, J. Electrochem. Soc. 150 (2) (2003) 176–192.
[11] S. Chen, C. Wan, Y. Wang, J. Power Sources 140 (September 2005) 111–124.
[12] A. Mills, S. Al-Hallaj, J. Power Sources 141 (2004) 207–315.
[13] U. Kim, J. Yi, C.B. Shin, T. Han, S. Park, J. Power Sources 196 (2011) 5115–5121.
[14] N. Nieto, L. Diaz, J. Gastelurrutia, I. Alava, F. Blanco, J. Ramos, A. Rivas, J. Electrochem. Soc. 160 (2) (November 2012) 212–217.
[15] Y. Ye, Y. Shi, A. Tay, J. Power Sources 217 (June 2012) 509–518.
[16] K. Lee, K. Smith, A. Pesaran, G. Kim, J. Power Sources (March 2013).
[17] S. Rickman, Orbital Thermal Environments Training, Thermal Fluids and Analysis Workshop, Pasedena, CA, 2011.
[18] Q. Wang, P. Ping, Z. Xuejuan, C. Guanquan, S. Jinhua, C. Chunhua, J. Power Sources 208 (2012) 210–224.
[19] H. Sun, X. Wang, B. Tossan, R. Dixon, J. Power Sources 206 (2012) 349–356.
[20] D.H. Jeon, S.M. Baek, Energy Convers. Manag. 52 (2011) 2973–2981.
[21] United States Air Force, Department of Defense Standard Practice: Product Verification Requirements for Launch, Upper Stage, and Space Vehicles, AMSC, 1999. FSE1810.